Int. J. Heat Mass Transfer. Vol. 33, No. 4, pp. 629–639, 1990
Printed in Great Britain

0017-9310/90 $3.00 + 0.00

Analytical and experimental study on turbulent natural convection in a horizontal annulus

KENJI FUKUDA, YASUTOMI MIKI and SHU HASEGAWA
Department of Nuclear Engineering, Faculty of Engineering, Kyushu University, Fukuoka 812, Japan

(*Received* 31 *March* 1989)

Abstract—A direct numerical simulation of the turbulent natural convection in a horizontal annulus is carried out using the explicit leap-frog scheme. The oscillatory flow as well as the turbulent flow are realized for Rayleigh numbers up to 6.0×10^5. The velocity and temperature profiles and their turbulent characteristics are also measured with a hot-wire anemometer and thermocouples, respectively. By carrying out the spectrum analysis of these data a transition from laminar to turbulent natural convection is clarified. Comparison between the experimental results and the analyses in terms of the average profiles and the turbulent quantities such as the turbulent intensities and the power spectra shows a good agreement.

1. INTRODUCTION

MANY WORKS have been conducted on natural convection in an annulus [1–11] including ours on three-dimensional steady and unsteady laminar flow using the finite difference method [1, 2] or the Galerkin method [3, 4]. The structure of the three-dimensional flow patterns as well as their transitions among static and/or dynamic modes are clarified using these methods.

Since the basic structures of the laminar natural convection have been well understood the concern is now being focused on turbulent or high-Rayleigh-number natural convection. Farouk and Guceri [11] carried out a numerical study for two-dimensional turbulent natural convection using the k–ε model. Though their results show good agreement with experimental data concerning average profiles of local Nusselt number more examinations on turbulent properties seem to be needed to confirm the model.

Owing to the recent development of supercomputers numerical analyses of the transient three-dimensional flow, which require an enormous number of grids and the consequent extremely large core size or CPU time, are becoming easier. In the field of Benard convection in a horizontal fluid layer even the turbulent three-dimensional flow is obtained [12] by simply solving the Navier–Stokes equation directly. It turned out that this method (direct numerical simulation or DNS) made it possible to simulate the turbulent natural convection not only in the inertial subrange but also in the molecular dissipation-dominant range. Oya *et al.* [13] also carried out the DNS of the turbulent flow in an annulus together with its experimental studies [14]. In this paper DNS is carried out for Rayleigh numbers up to 6.0×10^5 and the results are compared with the experimental ones to discuss the effectiveness or the limits of the DNS method.

2. NUMERICAL METHOD

Consider a fluid layer among two concentric horizontal cylinders of radii R_1, R_2 ($R_2 > R_1$), axial length λ, with surface temperatures T_1 and T_2 ($T_1 > T_2$), respectively, as shown in Fig. 1. In the analysis the Boussinesq approximation is assumed and the periodic boundary condition is applied in the axial direction. Introducing the following dimensionless time and coordinate denoted by a superscript *:

$$t^* = \alpha t/R_2^2, \quad r^* = r/R_2, \quad z^* = z/R_2,$$

$$u^* = R_2 u/\alpha, \quad T^* = (T-T_2)/(T_1-T_2),$$

$$p^* = p/\rho(\alpha/R_2)^2$$

the equations of conservation of mass, momentum and energy are written as follows (superscript * is omitted hereafter):

$$\nabla u = 0 \tag{1}$$

$$\partial u/\partial t = -\nabla p - (u\nabla)u + Pr\,\Delta u - Pr\,Ra\,Tc \tag{2}$$

$$\partial T/\partial t = -(u\nabla)T + \Delta T \tag{3}$$

where c is the direction cosine of the direction of

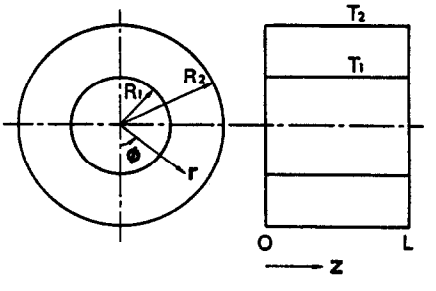

FIG. 1. Analytical model.

NOMENCLATURE

c	direction cosine of the direction of gravity	t	time
C_{rr}	axial cross correlation of radial velocity fluctuation	T	temperature
f	frequency	u	velocity
F_{rr}	one-dimensional energy spectrum defined by equation (7)	u_r'	radial velocity fluctuation
k_z	axial wave number	z	axial coordinate.
L	gap width of the annulus, R_2-R_1	Greek symbols	
p	pressure	α	thermal diffusivity
Pr	Prandtl number	λ	periodic length
r	radial coordinate	ρ	density
R	radius	ϕ	angular coordinate.
Ra	Rayleigh number	Subscripts	
R_{rr}	two-point correlation defined by equation (6)	r	radial
		z	axial
		ϕ	angular

gravity with its components

$$c_1 = \cos\phi, \quad c_2 = -\sin\phi, \quad c_3 = 0. \tag{4}$$

These equations are solved with the following boundary conditions:

$$u_r = u_\phi = u_z = 0 \quad (r = R_1, R_2)$$
$$T = 1 \quad (r = R_1)$$
$$T = 0 \quad (r = R_2)$$
$$\xi(r, \phi, 0) = \xi(r, \phi, \lambda) \quad (\xi = u, T, p) \tag{5}$$

which represent the non-slip condition on the cylinder walls as well as the periodic condition in the axial direction.

In the computation the explicit mixed, time-lagged leap-frog method as adopted by Grotzbach [12] is used for the time integration while the centered-space finite differential scheme is applied for the space integration. The Poisson equation, which is the result of taking the divergence of equation (2), is solved by the method of the fast Fourier transform (FFT). The staggered mesh system, which is uniform in the ϕ- and z-directions and nonuniform in the r-direction is adopted; it is taken denser for points closer to the walls to enable accurate calculation of steep distributions near the walls. To dampen the numerical oscillation of a period $2\Delta t$ inherent to the leap-frog method, the Euler type forward time differencing scheme is applied every 30 time steps.

3. EXPERIMENTAL APPARATUS

The experimental apparatus is shown in Fig. 2. This consists of a 112 mm o.d., 398 mm long, aluminum inner cylinder and a 224 mm i.d. copper outer cylinder with their end plates of 15 mm thick acrylic resin. The annulus between these cylinders is filled with air as the test fluid. The inner cylinder is heated by a heater placed inside it and the outer cylinder is cooled by water supplied from a chilling unit.

Sixteen A–C thermocouples are embedded to monitor and/or control the surface temperature of the cylinders and two pairs of 5 μm I-type tungsten KANOMAX hot-wire and 25 μm C–A thermocouples, which are inserted axially in holes bored through the end plates and can be traversed axially and rotated azimuthally, are utilized to measure the temperature and the velocity field. This thermocouple is placed 1 mm downstream from the hot wire and is used to compensate the temperature effect of the hot-wire signal. The angle of the hot wire is such that the wire is normal to the direction of the flow and its signal shows a maximum. These data are taken with the data acquisition system (HP-3497A) and are dealt with using the FACOM VP-100 supercomputer.

The error in measuring the very low flow velocity with the hot wire is evaluated as follows. (i) Compensation of the temperature effect using the temperature measured at a point 1 mm from the hot wire may cause an error, depending on the temperature gradient, typically of the order of 1 cm s^{-1} at the top of the annulus at $r = 0.56$, $Ra = 10^5$. (ii) The error in the calibration curve for the hot wire, which was taken at room temperature, and those in measuring the temperature as well as the velocity itself may cause a 10% error. (iii) The electric resistance of connecting wires is affected by a change in room temperature, causing an estimated error within 5%. On the whole, the maximum error is assumed to be 30%, which is larger for smaller velocities.

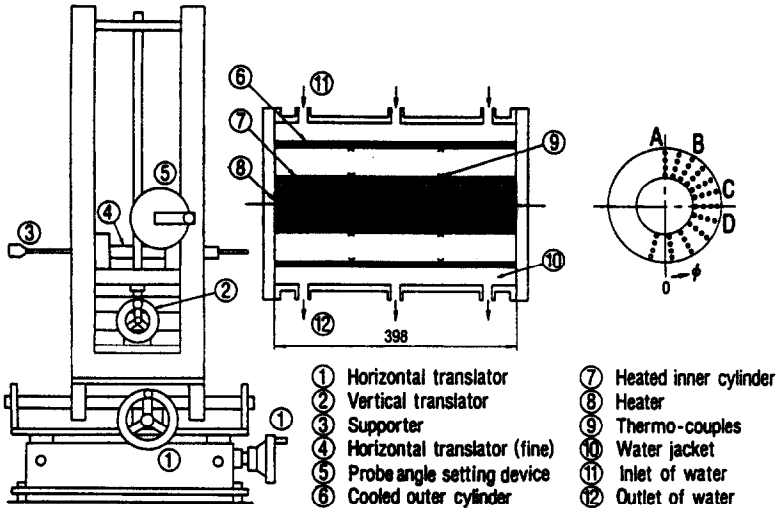

FIG. 2. Experimental apparatus.

4. RESULTS AND DISCUSSIONS

4.1. *Parameters for numerical analysis*

Analyses are carried out for a fixed aspect ratio $R_1/R_2 = 0.5$, an axial length of periodicity $\lambda = 2.8(R_2 - R_1)$ and $Pr = 0.71$ for the Rayleigh number range $Ra = 4 \times 10^3$–6×10^5. To save computation time, a conduction dominant temperature distribution was first obtained, and the solution for higher Ra was obtained successively using the solution for Ra just below it as the initial value. Time required for computation of one time step in the case of the typical number of grids $17 \times 96 \times 32$ along the radial, circumferential and axial coordinates, respectively, was about 0.3 s.

The number of grids together with other parameters for computation are shown in Table 1, where Nusselt numbers represent average values of those at the inner and outer cylinders, which are within the relative error of 3% showing a good heat balance between these cylinders. Steady-state solutions for cases 1–4 while unsteady solutions for cases 5–8 were attained as a large number of time steps elapsed.

4.2. *Steady flow and oscillatory flow*

Three-dimensional steady-state characteristics were widely studied analytically and experimentally in our previous works [1, 2, 4] with which the validity of the analytical code utilized here was examined. Thus duplication is prevented and only a comparison in terms of the average Nusselt number is given in Fig. 3. It is found that Itoh *et al.*'s [15] correlation agrees well with the analytical results especially in a two-dimensional stable flow region.

When the Rayleigh number is increased the flow becomes unstable and the oscillatory flow appears. As a result the average Nusselt number fluctuates on both cylinder surfaces, with a bigger amplitude on the outer cylinder, and a plume generated at the top of the annulus oscillating right and left. Figure 4 shows the analytical temperature distributions for various Rayleigh numbers. As observed by Bishop *et al.* [9], this fluctuation of the plume is a three-dimensional phenomenon and the axial distributions of the temperature and the velocity contours are wavy and seem to be moving axially. As the Rayleigh number is increased further the oscillatory flow gradually loses

Table 1. Analytical parameters and result of mean Nusselt number (error denotes discrepancy of Nu between the outer and inner cylinder surfaces)

No.	Ra_L	Mesh	Dt	Nu (error)
1	4.0×10^3	$11 \times 48 \times 20$	2.0×10^{-4}	1.477 (0.06%)
2	2.0×10^4	$11 \times 48 \times 20$	1.0×10^{-4}	2.509 (0.13%)
3	6.0×10^4	$11 \times 96 \times 20$	5.0×10^{-5}	3.015 (2.83%)
4	1.0×10^5	$11 \times 96 \times 20$	5.0×10^{-5}	3.522 (1.99%)
5	1.1×10^5	$17 \times 96 \times 32$	2.5×10^{-5}	3.607 (0.15%)
6	1.5×10^5	$17 \times 96 \times 32$	2.5×10^{-5}	3.975 (0.06%)
7	3.0×10^5	$17 \times 96 \times 32$	2.5×10^{-5}	5.012 (0.81%)
8	6.0×10^5	$17 \times 96 \times 32$	2.5×10^{-5}	6.027 (1.68%)

$R_1/R_2 = 0.5$; periodic length, $2.8(R_2 - R_1)$; $Pr = 0.71$.

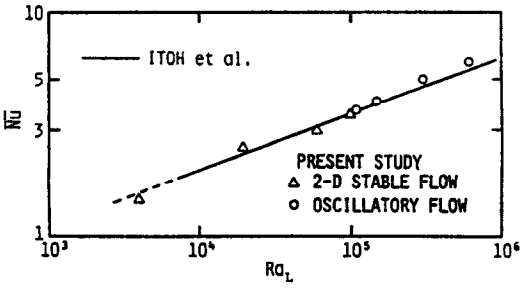

FIG. 3. Comparison of analytical mean Nusselt numbers and Itoh *et al.*'s correlation [15].

its periodicity and shows turbulent features. For $Ra > 3 \times 10^5$ the flow patterns are apparently irregular and will be treated statistically.

4.3. *Turbulent flow*

4.3.1. *Temperature fluctuations and power spectrum.* The experimental and analytical results of temperature fluctuations are compared in Fig. 5. The difference in axial position has a negligible effect for this comparison because of the periodic condition along the z-axis in the analysis which is a good approximation of the infinite system free from the effect of the rigid end walls. For convenience, the dimensionless time may be multiplied by 550 to obtain the actual time in seconds.

It is shown that the periodic temperature oscillations for lower Rayleigh numbers are simulated well by the analysis, except that their amplitudes are larger than the experimental results. This may be due to the following reasons. Because of the periodic boundary condition restriction on the movement of the fluid due to the viscous shear stress on the end walls does not exist, which will result in the larger amplitude of oscillation. The analysis also predicts well the irregular fluctuations for higher Rayleigh numbers and their amplitude as well. Since the scale of vortices, which typically represent the flow structure, becomes small enough the presence of the end walls has no effect and the periodic boundary condition may be appropriately applied.

The power spectra of these temperature fluctuations are obtained with the maximum entropy method and compared in Fig. 6. It is shown that, as Ra_L is increased, the peaks in the spectrum move toward the higher frequency side and the spectrum itself gradually changes from a line spectrum to a continuous one. This trend corresponds to the transition from the laminar to the turbulent flow. It should also be noted that the slope of the decrease of the spectrum is smaller and that the magnitude of $P(f)$ is larger in the analysis, indicating the existence of a greater number of high-frequency components. As the time mesh 2.5×10^{-5} corresponds to the dimensionless frequency $f = 4 \times 10^4$ thus $f = 300$ to 0.55 Hz, neither to the limit of computation due to the size of the time mesh nor to the limit of measurement due to the time constant of the thermocouple are attributed this discrepancy. However, the aliasing error which inherently results from the digital, finite difference method, will produce high frequency components in the flow field and this is assumed to be a reason.

4.3.2. *Velocity fluctuation and its power spectrum.* Velocity fluctuations and their power spectra obtained experimentally and analytically are compared in Figs. 7 and 8. Similarly to the case of temperature fluctuation it is noted that the analysis predicts well the trend of velocity fluctuation, but with slightly bigger amplitudes of fluctuations at lower Rayleigh numbers and smaller time-averaged velocity at $Ra_L = 6 \times 10^5$ (Fig. 7).

Comparison of the power spectrum also shows a very good correspondence. The positions of the peaks typically for the case of $Ra_L = 1.1 \times 10^5$ are 0.128, 0.254 and 0.380 Hz in the experiment, showing the frequencies of the fundamental mode and its harmonics, and are 0.118, 0.228 and 0.336 Hz in the analysis. The agreement is satisfactory and thus the validity of the analysis is confirmed. It is found that, as Ra_L is

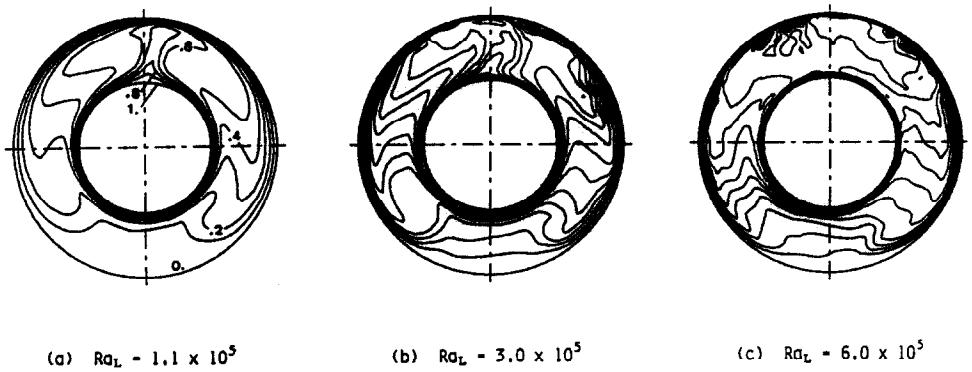

FIG. 4. Instantaneous temperature distributions at $z/\lambda = 7/32$ (the spacings between isotherms are $\Delta T = 0.1$ for (a) and 0.05 for (b) and (c)).

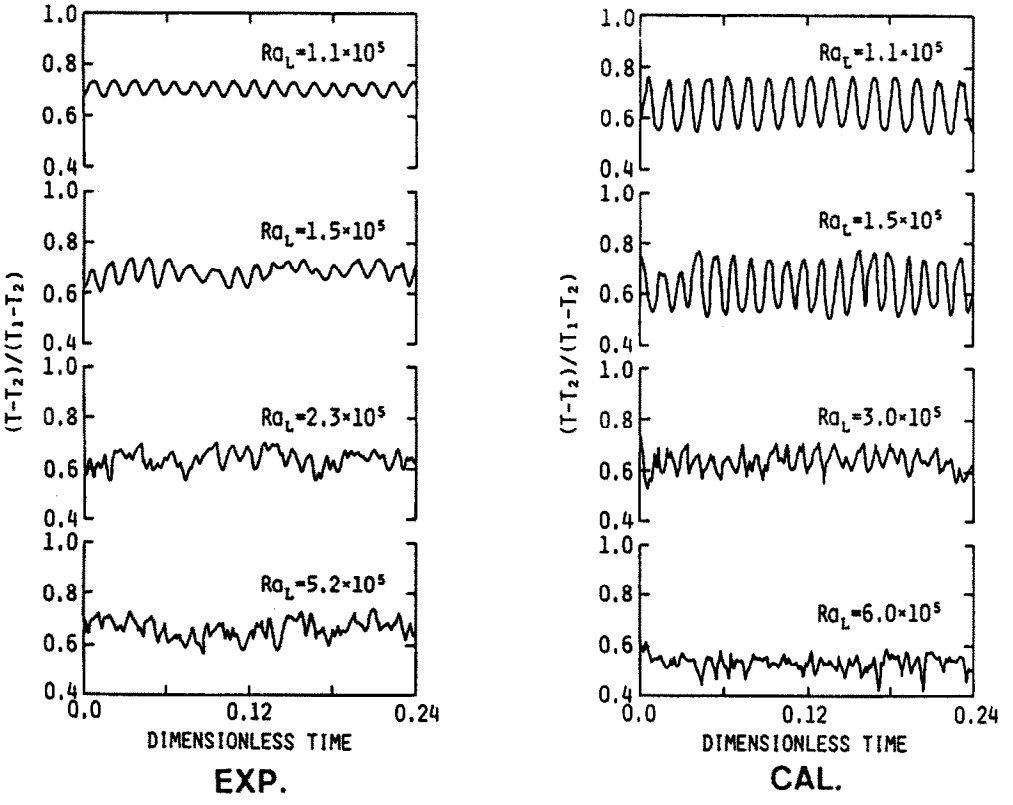

FIG. 5. Comparison between experimental and analytical temperature fluctuations (EXP—experimental, $r = 0.81$, $\phi = 178$ deg at axial center; CAL—analytical, $r = 0.7875$, $\phi = 174.375$ deg, $z/\lambda = 7/32$).

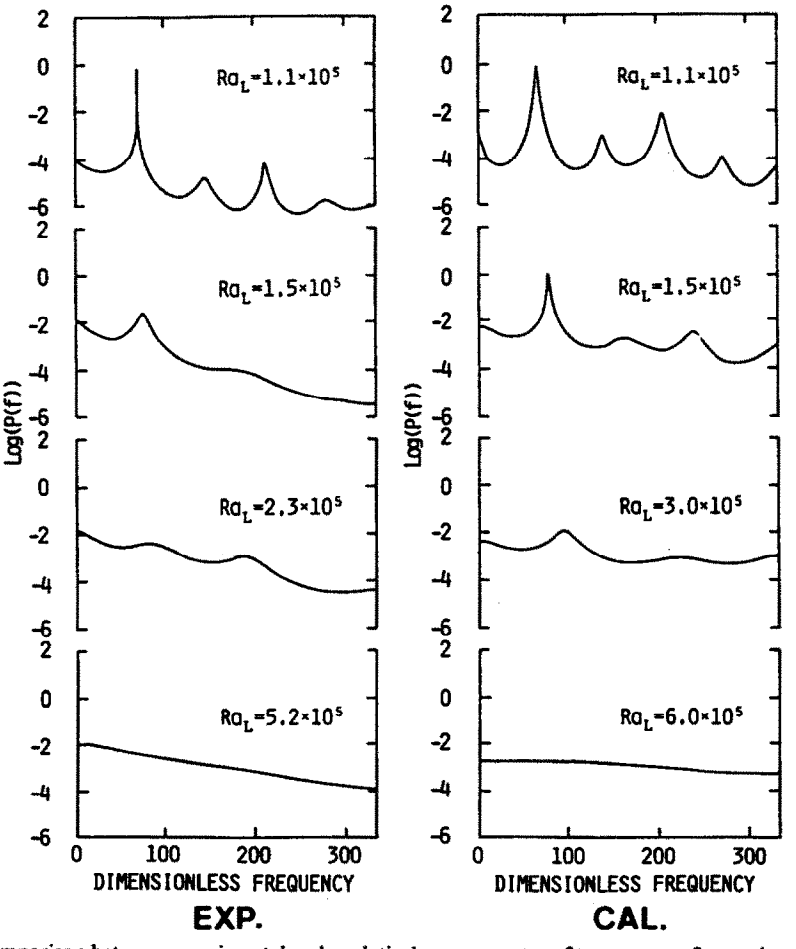

FIG. 6. Comparison between experimental and analytical power spectra of temperature fluctuations shown in Fig. 5.

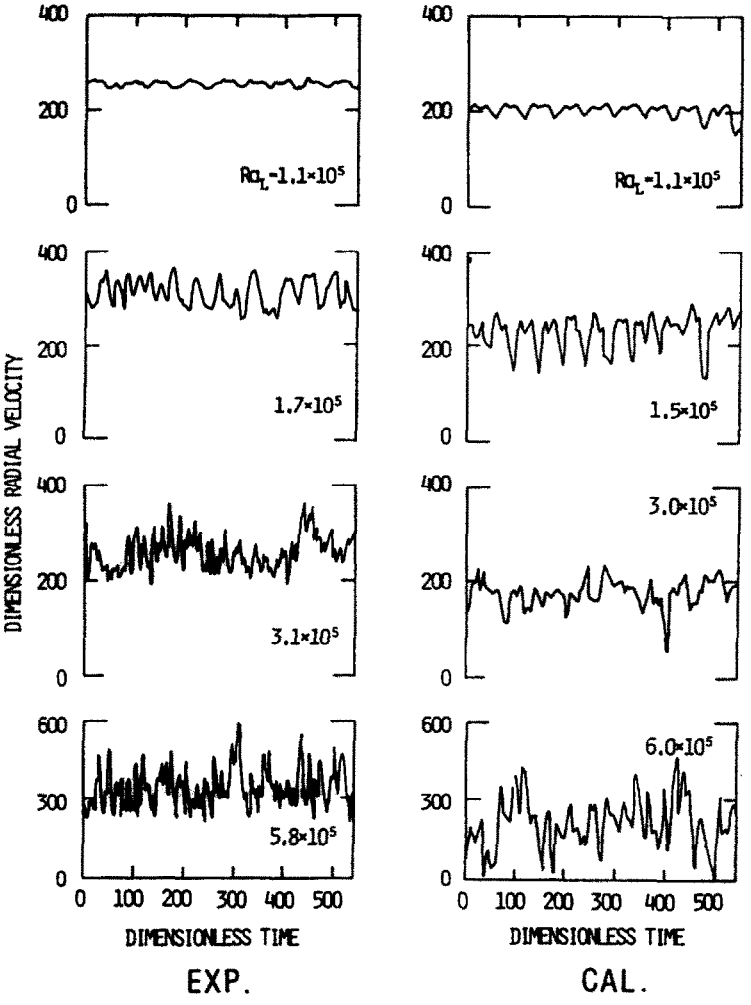

FIG. 7. Comparison between experimental and analytical velocity fluctuations (EXP—experimental; CAL—analytical, $r = 0.688$, $\phi = 180$ deg at axial center).

increased, the positions of the peaks move toward the higher frequency side and that the spectrum changes from a line spectrum to a continuous one; which is the same as the case of the temperature spectrum shown in Section 4.3.1. Contrary to the temperature case, some weak peaks remain even if Ra_L is increased to 6.0×10^5, which might indicate the existence of some bigger structural flow than of the homogeneous flow.

4.3.3. *Period of the fundamental mode.* The period of oscillation of the fundamental mode for temperature and velocity fluctuations are plotted against Ra_L in Fig. 9 which shows very good agreement with each other. The lower Rayleigh number limit at which the flow is unsteady is around 6×10^4 as observed by Powe *et al.* [8]. The upper limits of Ra_L for the distinguishable fundamental mode are 3.6×10^5 experimentally and 3.0×10^5 analytically.

4.3.4. *Time-averaged temperature and velocity distributions.* Temperature and velocity distributions were measured for $Ra_L = 5.2 \times 10^4 \sim 9.2 \times 10^5$, at $\phi = 75$, 105, 150 and 180 deg each at $r = 0.563$, 0.688, 0.813 and 0.938 or at 16 points altogether; these are located at the axial center. Since the hot wire for the velocity measurement is placed on the place normal to the axis and is rotated such that its signal shows a maximum, the distribution obtained at $\phi = 180$ deg is compared with the analytical u_r and others are compared with distributions of u_ϕ. This comparison is based on an assumption that the effect of other velocity components is small.

Time-averaged temperature and velocity distributions are shown in Figs. 10 and 11. A very good coincidence between experiment and analysis in Fig. 10 and a qualitative agreement in Fig. 11 are observed except for the case of $Ra_L = 6 \times 10^5$. In this last case the analysis predicts more turbulent flow with more uniform temperature distribution than the experiment. On the other hand, in the experiment a plume-like flow still exists at the top of the annulus though the

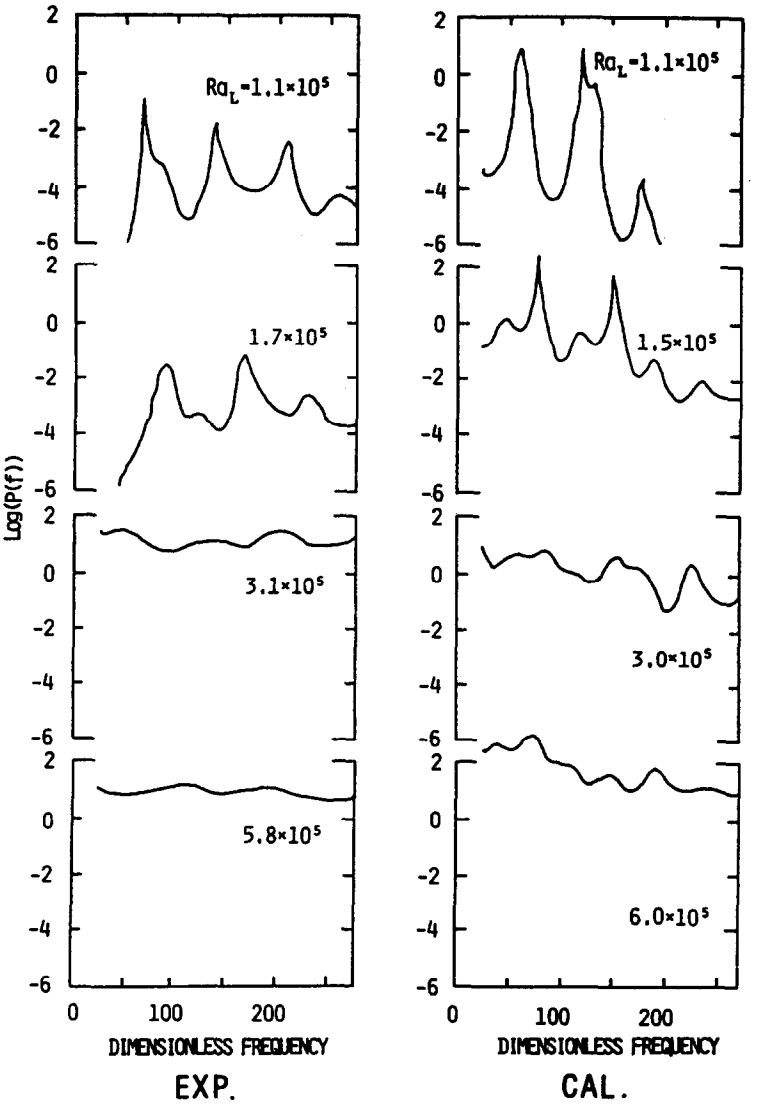

FIG. 8. Comparison between experimental and analytical power spectra of velocity fluctuations shown in Fig. 7.

'flattening' process takes place in the other portion. It is also found that the boundary-layer-like flow adjacent to the cylinder walls develops as Ra_L increases.

Grotzbach [12] points out that the DNS tends to predict more turbulent flow if it fails to simulate the dissipation dominant frequency zone. As this is the case in this analysis, the disagreement for the case of $Ra_L = 6 \times 10^5$ might be ascribed to the limit of the analysis. Also, in the experiment in this case, the temperature difference between the outer and inner cylinders is so large (up to 50°C) that it is suspected that the Boussinesq approximation, which this analysis is based on, is not valid.

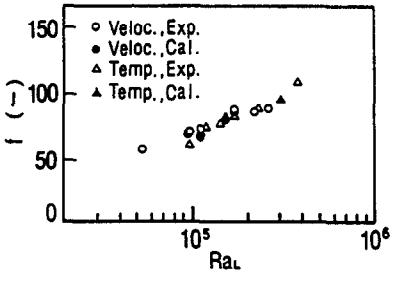

FIG. 9. Comparison between experimental and analytical periods of fundamental modes derived from Figs. 6 and 8.

4.3.5. *Intensity of turbulence.* The r.m.s. values of temperature and velocity variations (intensities) are shown in Figs. 12 and 13. One may find a fairly good agreement within the error discussed in Section 3 between experiment and analysis in Fig. 13 except for the case of $Ra_L = 6 \times 10^5$ and in Fig. 12 for high Ra_L. It is also noted that the magnitude of the temperature fluctuation at the top of the annulus ($\phi = 180$ deg) around $r = 0.8$ is rather large for low Rayleigh num-

Table 2. Symbols used in Figs. 10 and 12

Exp.	Cal.	ϕ (deg)
□	———	75
△	- - - -	105
▽	-------	150
○	———	180

bers, while it is exceeded by those at other portions thus resulting in the apparent change in the shape of the distribution.

On the other hand, the velocity fluctuation is small for low Rayleigh numbers, but increases dramatically near the cylinder walls and as a consequence the shape of the distribution changes. Since it is observed that the sharp peaks in the power spectra disappear at

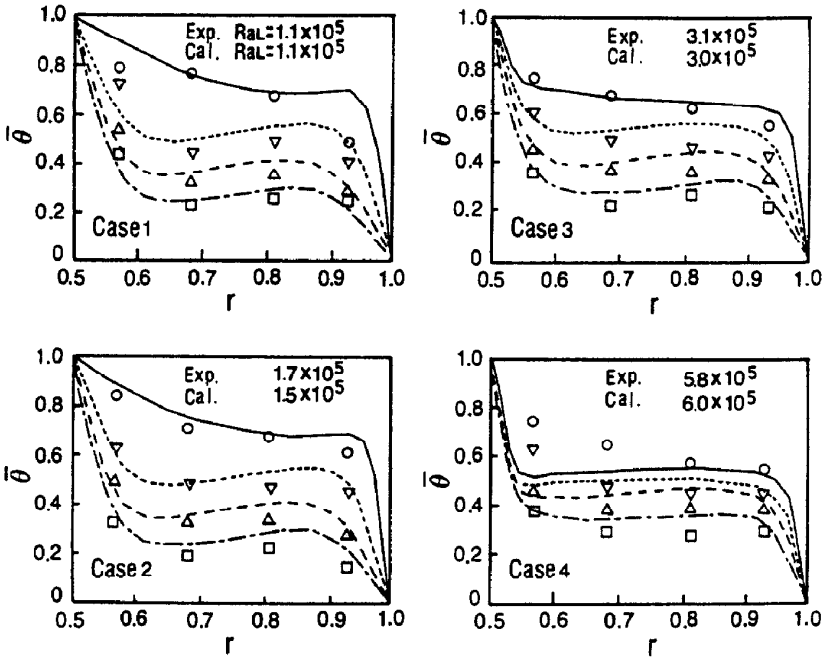

FIG. 10. Comparison between experimental and analytical time-averaged temperature distributions (see Table 2 for symbols).

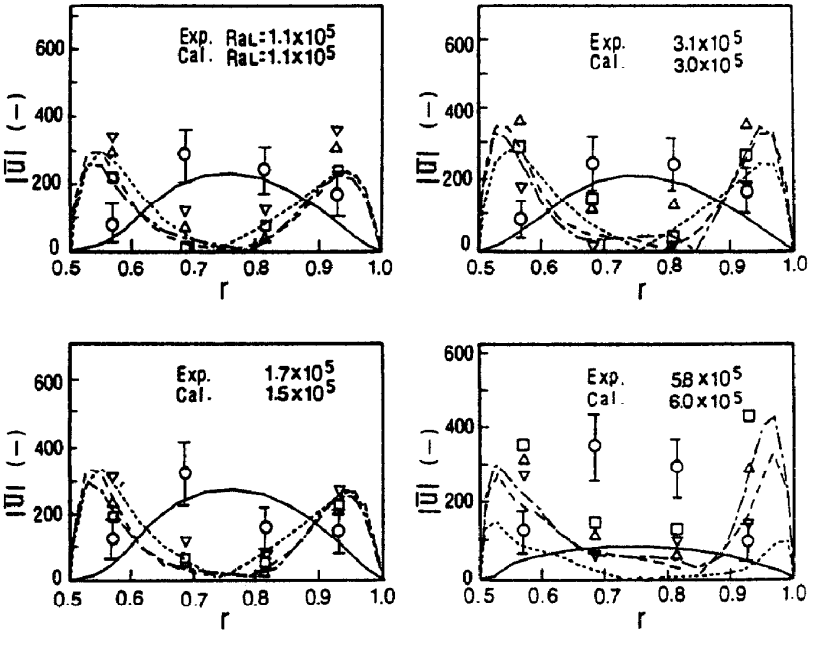

FIG. 11. Comparison between experimental and analytical time-averaged velocity distributions (see Table 3 for symbols).

Table 3. Symbols used in Figs. 11 and 13

u	Exp.	Cal.	ϕ (deg)
u_ϕ	□	——	75
u_ϕ	△	- - - -	105
u_ϕ	▽	-------	150
u	○	———	180

around $Ra_L = 3 \times 10^5$ and it becomes difficult to define the fundamental period (cf. Figs. 7–9), it is assumed that the flow becomes turbulent at this critical Rayleigh number.

4.3.6. *Cross-correlation of velocity variation.* Velocity fluctuation is measured at two axially separate points simultaneously using a pair of two hot wires, from which a cross-correlation defined by equation

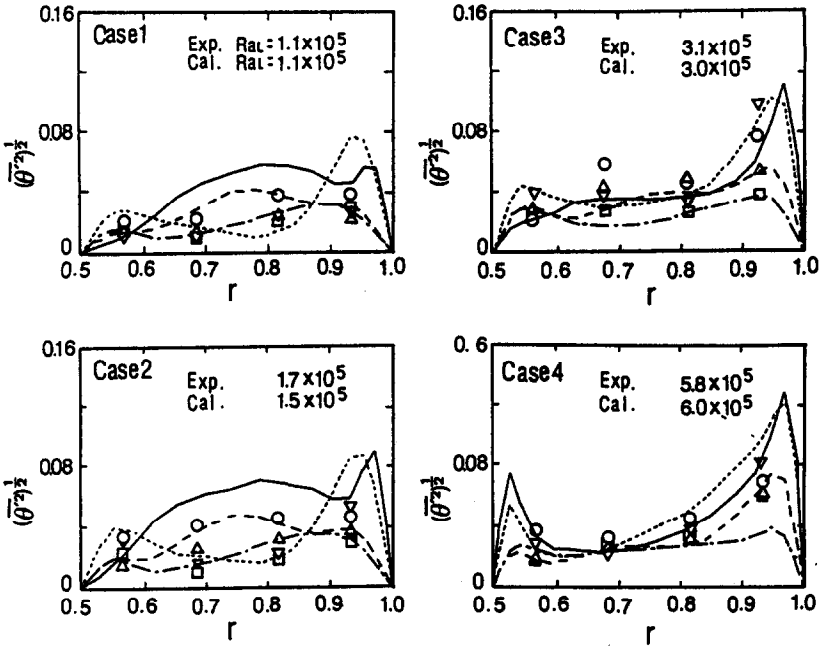

FIG. 12. Comparison between experimental and analytical r.m.s. values of temperature fluctuations (see Table 2 for symbols).

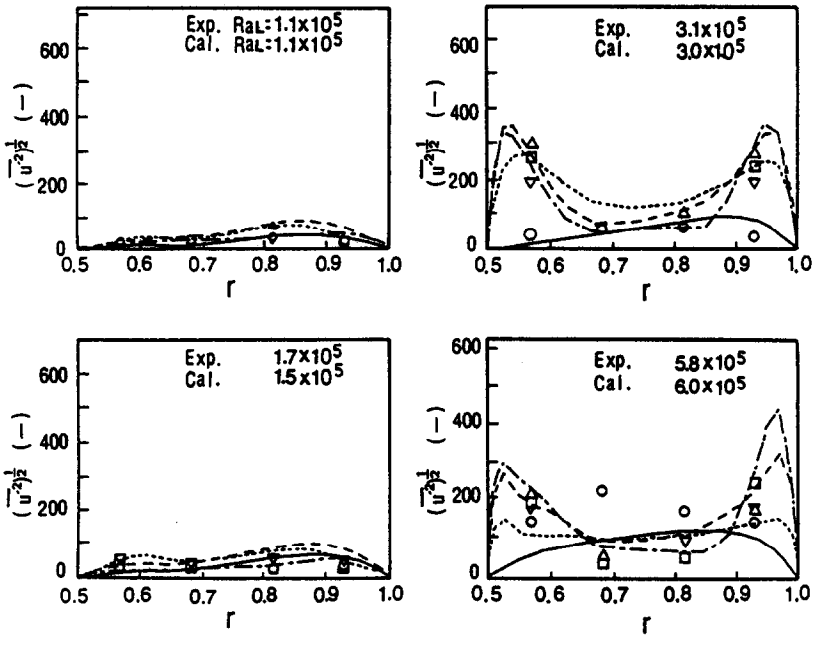

FIG. 13. Comparison between experimental and analytical r.m.s. values of velocity fluctuations (see Table 3 for symbols).

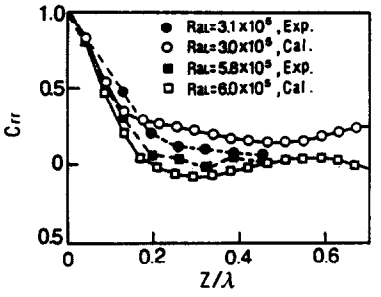

FIG. 14. Comparison between experimental and analytical axial two-point correlations of velocity fluctuations at $r = 0.688$, $\phi = 180$ deg.

(6) is evaluated

$$C_{rr}(z) = R_{rr}(z)/R_{rr}(0)$$
$$R_{rr}(z) = u_r'(z_0+z). \qquad (6)$$

The experimental results thus obtained are compared with the analytical results in Fig. 14 which shows good agreement. It is noted that the cross-correlation decreases to almost zero at $z/\lambda = 0.2 \sim 0.5$ or $z = 0.6 \sim 1.4(R_2 - R_1)$ indicating that the largest vortices lie around this value. As is expected, this characteristic scale decreases as Ra_L increases.

4.3.7. *Energy spectrum.* The analytical one-dimensional energy spectrum of u_r' in the z-direction $F_{rr}(k_z)$ defined by equation (7) is shown in Fig. 15

$$F_{rr}(k_z) = \int_{-\infty}^{\infty} \exp(-ik_z z) R_{rr}(z)\, dz/2\pi. \qquad (7)$$

It is found that the magnitude of the energy spectrum is larger for vortices which are nearer to the top of the annulus, drops sharply with increasing wave number and is shifted up if Ra_L is increased especially for portions at higher wave number; i.e. the contribution from the small vortices increases. This indicates that the intensity of the turbulence is highest at the top of the annulus and that it tends to grow more rapidly at lower positions to achieve a more uniform distribution as Ra_L increases. It seems that the spectrum has an asymptote with a slope of $-5/3$ suggesting the existence of the so-called inertial subrange. For the spectrum of higher wave numbers it is expected to have a far steeper slope. Unfortunately due to the limit of the analysis this spectrum zone is not simulated.

5. CONCLUDING REMARKS

Direct numerical simulation (DNS) of the turbulent natural convection in a horizontal annulus is carried out to obtain temperature and velocity profiles and their turbulent quantities. By comparing these results with experiments validity and limitation of the DNS are clarified. A few concluding remarks are given as follows.

(1) With increasing Rayleigh number, the stable flow pattern changes into the periodic one and then the irregular turbulent flow appears. This general trend is well simulated by the DNS.

(2) The DNS simulates the mean temperature and the velocity profiles well except for the case of high Ra where the Boussinesq approximation might not be adequate.

(3) In terms of the power spectrum and the period of flow oscillation the experiment and the DNS show a good coincidence.

(4) Comparison of experimental and numerical turbulent quantities such as intensities of velocity and temperature fluctuations shows a good agreement within an experimental error.

(5) Due to the restriction of the number of the grid the dissipation dominant profile in the energy spectrum is hardly simulated completely and as a result the turbulent quantities seem to be overestimated.

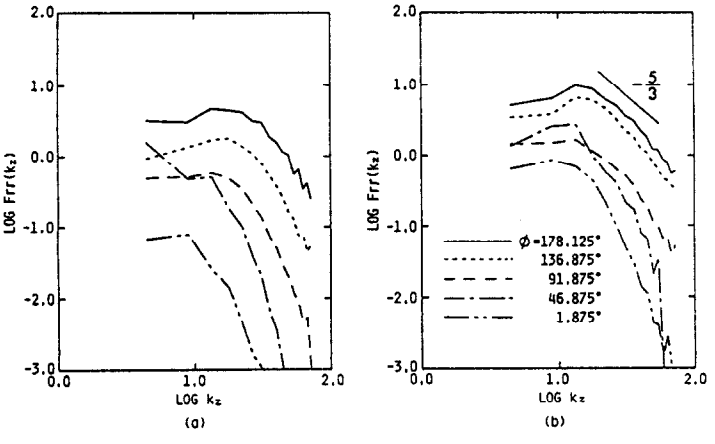

FIG. 15. One-dimensional energy spectra: (a) $Ra_L = 3.0 \times 10^5$; (b) $Ra_L = 6.0 \times 10^5$.

Acknowledgement—The authors would like to express their appreciation to Mr T. Oya and Mr K. Morita for their help. This study is partly supported by Japan Atomic Energy Research Institute (JAERI) under Grant No. 87137. The numerical work was conducted using the supercomputers in the Computing Center of Kyushu University and in JAERI.

REFERENCES

1. Y. Takata, K. Iwashige, K. Fukuda and S. Hasegawa, Three-dimensional natural convection in an inclined cylindrical annulus, *Int. J. Heat Mass Transfer* **27**, 747–754 (1984).
2. Y. F. Rao, Y. Miki, K. Fukuda, Y. Takata and S. Hasegawa, Flow patterns of natural convection in horizontal cylindrical annuli, *Int. J. Heat Mass Transfer* **28**, 705–714 (1985).
3. Y. F. Rao, K. Fukuda and S. Hasegawa, Steady and transient analyses of natural convection in a horizontal porous annulus with Galerkin method, *J. Heat Transfer* **109**, 919–927 (1987).
4. Y. F. Rao, K. Fukuda and S. Hasegawa, A numerical study of three-dimensional natural convection in a horizontal porous annulus with Galerkin method, *Int. J. Heat Mass Transfer* **31**, 695–707 (1988).
5. J. P. Caltagirone, Thermoconvective instabilities in a porous medium bounded by two concentric horizontal cylinders, *J. Fluid Mech.* **76**(2), 337–362 (1976).
6. U. Grigull and W. Hauf, Natural convection in horizontal cylindrical annuli, *Proc. 3rd Int. Heat Transfer Conf.*, Vol. 2, pp. 182–195 (1966).
7. C. Liu, W. K. Mueller and F. Landis, Natural convection heat transfer in long horizontal cylindrical annuli, *Int. Dev. Heat Transfer* **5**, 976–984 (1961).
8. R. E. Powe, C. T. Carley and S. L. Carruth, A numerical solution for natural convection in cylindrical annuli, *Trans. ASME, J. Heat Transfer* **92**, 210–219 (1971).
9. E. H. Bishop, C. T. Carley and R. E. Powe, Natural convective oscillatory flow in cylindrical annuli, *Int. J. Heat Mass Transfer* **11**, 1741–1752 (1968).
10. T. H. Kuehn and R. J. Goldstein, An experimental and theoretical study of natural convection in the annulus between horizontal concentric cylinders, *J. Fluid Mech.* **74**(4), 695–719 (1976).
11. B. Farouk and S. I. Guceri, Laminar and turbulent natural convection in the annulus between horizontal concentric cylinders, *J. Heat Transfer* **104**, 631–636 (1982).
12. G. Grotzbach, Direct numerical simulation of laminar and turbulent Benard convection, *J. Fluid Mech.* **119**, 27–53 (1982).
13. T. Oya, Y. Miki, K. Morita, K. Fukuda and S. Hasegawa, Unsteady three-dimensional behavior of natural convection in horizontal annulus, *J. Atom. Energy Soc. Japan* **30**(1), 87–96 (1988).
14. Y. Miki, T. Oya, K. Morita, K. Fukuda and S. Hasegawa, Unsteady three-dimensional behavior of natural convection in horizontal annulus (II), *J. Atom. Energy Soc. Japan* **30**(2), 172–189 (1988).
15. M. Itoh, T. Fujita, N. Nishiwaki and M. Hirata, A new method of correlating heat transfer coefficients for natural convection in horizontal cylindrical annuli, *Int. J. Heat Mass Transfer* **13**, 1364–1368 (1970).

ETUDE ANALYTIQUE ET EXPERIMENTALE DE LA CONVECTION NATURELLE TURBULENTE DANS UN ESPACE ANNULAIRE HORIZONTAL

Résumé—Une simulation numérique directe de la convection naturelle turbulente dans un espace annulaire horizontal est conduite en utilisant un schéma explicite à "saut de grenouille". L'écoulement oscillatoire aussi bien que l'écoulement turbulent sont réalisés pour des nombres de Rayleigh jusqu'à $6{,}0 \times 10^5$. Les profils de vitesse et de température et leurs caractéristiques turbulentes sont aussi mesurés avec un anémomètre à fil chaud et des thermocouples. En faisant l'analyse spectrale de ces données on précise la transition entre convection laminaire et turbulente. On obtient un bon accord dans la comparaison entre les résultats expérimentaux et les analyses en ce qui concerne les profils moyens et les grandeurs turbulentes telles que les intensités turbulentes et le spectre de puissance.

ANALYTISCHE UND EXPERIMENTELLE UNTERSUCHUNG DER TURBULENTEN NATÜRLICHEN KONVEKTION IN EINEM WAAGERECHTEN RINGRAUM

Zusammenfassung—Die turbulente natürliche Konvektion in einem waagerechten Ringraum wird mit Hilfe des expliziten Durchprüfungsverfahrens direkt numerisch simuliert. Die schwingende und die turbulente Strömung werden für Rayleigh-Zahlen bis 6×10^5 wiedergegeben. Geschwindigkeits- und Temperaturprofile und ihr turbulentes Verhalten wurden außerdem mit einem Hitzdrahtanemometer bzw. mit Thermoelementen gemessen. Mit Hilfe einer Spektralanalyse dieser Daten wurde der Übergang von laminarer zu turbulenter natürlicher Konvektion klargestellt. der Vergleich zwischen experimentellen Ergebnissen und der theoretischen Untersuchung zeigt bezüglich der mittleren Verläufe und der Turbulenzgrößen wie Turbulenzgrad und Leistungsspektrum gute Übereinstimmung.

АНАЛИТИЧЕСКОЕ И ЭКСПЕРИМЕНТАЛЬНОЕ ИССЛЕДОВАНИЕ ЕСТЕСТВЕННОЙ ТУРБУЛЕНТНОЙ КОНВЕКЦИИ В ГОРИЗОНТАЛЬНОМ КОЛЬЦЕВОМ КАНАЛЕ

Аннотация—С использованием явной схемы "чехарды" проводится прямое численное моделирование естественной турбулентной конвекции в горизонтальном кольцевом канале. Экспериментально реализованы колебательное, а также турбулентное течения при числах Рэлея вплоть до $6{,}0 \times 10^5$. С применением термоанемометра и термопар измерены соответственно профили скоростей и температур, а также их турбулентные характеристики. При помощи спектрального анализа этих данных выявлен переход от ламинарной к турбулентной естественной конвекции. Результаты эксперимента хорошо согласуются с анализом в терминах средних профилей таких турбулентных величин, как интенсивность турбулентности и энергетический спектр.